Biosensors and Bioelectronics 144 (2019) 111626

Contents lists available at ScienceDirect

Biosensors and Bioelectronics

journal homepage: www.elsevier.com/locate/bios

Intracellular cardiomyocytes potential recording by planar electrode array and fibroblasts co-culturing on multi-modal CMOS chip

Jong Seok Park[a,1], Sandra I. Grijalva[b,1], Doohwan Jung[a], Sensen Li[a], Gregory V. Junek[a], Taiyun Chi[a], Hee Cheol Cho[b,**], Hua Wang[a,*]

[a] School of Electrical and Computer Engineering, Georgia Institute of Technology, Atlanta, GA, USA
[b] Department of Biomedical Engineering, Emory University, Atlanta, GA, USA

ARTICLE INFO

Keywords:
Intracellular action potential recording
Cardiomyocytes
CMOS
Multimodality sensor array
Cellular impedance sensing
Drug screening

ABSTRACT

Intracellular action potential signals reveal enriched physiological information. Patch clamp techniques have been widely used to measure intracellular potential. Despite their high signal fidelity, they suffer from low throughput. Recently, 3D nanoelectrodes have been developed for intracellular potential recording. However, they are limited by scalability, yield, and cost, directly constraining their use in monitoring large number of cells and high throughput applications. In this paper, we demonstrate intracellular potential monitoring of cardiomyocytes using simple 2D planar electrode array in a standard CMOS process without patch clamps or post fabricated 3D nanoelectrodes. This is enabled by our unique cardiomyocytes/fibroblasts co-culturing technique and electroporation. The co-cultured fibroblasts promote tight sealing of cardiomyocytes on electrodes and enable high-fidelity intracellular potential monitoring based on 2D planar electrode. Compared to existing technologies, our platform has a unique potential to achieve an unprecedented combination of throughput, spatiotemporal resolution, and a tissue-level field-of-view for cellular electrophysiology monitoring.

1. Introduction

Intracellular electrochemical monitoring reveals enriched physiological information which has propelled major scientific progress in electrophysiology and many biotechnologies. In particular, the intracellular recordings of cardiomyocytes and neurons show a full amplitude and shape of the action potential and disclose enriched information on the activity of ion channels. Patch clamp techniques have been widely used to measure transmembrane potential by directly inserting a glass micropipette into the cell (Sakmann and Neher, 1984, 2009). With its high signal-to-noise ratio (SNR), temporal resolution, and signal fidelity, patch clamp measurements are often considered as the golden standard for intracellular action potential recording. However, due to their large form-factor, patch clamps suffer from limited throughput and poor scalability to massively paralleled monitoring. For example, it is difficult to employ many patch clamps concurrently on the same cell aggregates or tissues to capture the cellular network behaviour. Furthermore, due to their intrinsic invasiveness, patch clamps may affect the intracellular fluid balance and pose challenges for long-term intracellular monitoring.

Recently, a variety of vertical 3-dimensional (3D) nanoelectrode arrays have been demonstrated with the ability to measure intracellular potentials of in vitro cultured cardiomyocytes and neurons to improve spatial resolution and throughput over patch clamp techniques (Lin et al., 2014; Xie et al., 2012; Dipalo et al., 2017; Duan et al., 2012; Tian et al., 2010; Hai et al., 2010; Spira et al., 2013; Abbott et al., 2017; Shalek et al., 2010; Robinson et al., 2012). The cell-to-electrode interface conditions, often modelled as an interface junctional membrane impedance and a surrounding sealing resistance, are critical for intracellular potential recording (Spira et al., 2013; Asphahani et al., 2007). The 3D nanoelectrodes promote spontaneous membrane porations caused by very thin and extremely sharp nanostructures, e.g., a nanowire with the diameter of 150 nm and the height of 3 μm (Robinson et al., 2012). Thus, the nanoelectrodes can be engulfed by cells, which disrupts cell membranes and enables intracellular potential measurements. So far, most research efforts focus on improving these cell-to-electrode interfaces, essentially, lowering the junctional membrane impedance and increasing the surrounding sealing resistance. Thus, various 3D nanoelectrode structures including nanotubes (Lin et al., 2014), nanopillars (Xie et al., 2012), mushroom-shaped

* Corresponding author. Georgia Institute of Technology, 777 Atlantic Drive, N.W, Atlanta, GA, 30332-0250, USA.
** Corresponding author. Emory University, 1760, Haygood Dr. NE, Atlanta, GA, 30322, USA.
E-mail addresses: heecheol.cho@emory.edu (H.C. Cho), hua.wang@ece.gatech.edu (H. Wang).
[1] co-first author.

https://doi.org/10.1016/j.bios.2019.111626
Received 10 June 2019; Received in revised form 11 August 2019; Accepted 21 August 2019
Available online 28 August 2019
0956-5663/

electrodes (Hai et al., 2010), and nanowires (Abbott et al., 2017; Shalek et al., 2010; Robinson et al., 2012) have been developed to improve cell-to-electrode interface.

Recently, field effect transistor (FET) coupled 3D vertical nanoelectrodes (Duan et al., 2012; Tian et al., 2010) have been explored to further improve the signal-to-noise ratio and to realize multiplexing operations for addressability. 3D vertical nanoelectrodes are post-fabricated on 2D microelectrode arrays implemented in standard CMOS processes, in order to achieve close-in and low-noise readout by utilizing the underlying CMOS analog/digital circuitry (Abbott et al., 2017). However, 3D vertical nanoelectrodes require highly involved and often low-yield fabrication steps, resulting in substantial post-fabrication investment on CMOS microelectrode array (MEA) chips. In particular, a high-yield post fabrication of 3D vertical nanoelectrodes on high density CMOS MEA array ($>$ 10,000 electrodes and electrodes size $<$ 10μm $\times$ 10 μm) is especially difficult. Moreover, junctional membrane impedance reduction with 3D vertical nanoelectrodes is often limited, necessitating an additional electroporation/optoporation techniques. In addition, since metal-coated 3D vertical nanoelectrodes present excessively small surface areas, the electrode-electrolyte interface impedance is often very high, e.g., $\approx$100 GΩ at 1Hz (Abbott et al., 2017), causing significant signal-to-noise ratio degradation in recording and undesired faradaic reaction by the electrical pulses in electroporation. For successful intracellular potential recordings, cells should tightly engulf sharp 3D vertical nanoelectrodes with stable internalization, and this stringent cell-to-nanoelectrode interface requirement makes cell culturing/patterning, surface treatment, and long-term recording challenging. Also, the 3D vertical nanoelectrodes intrinsically disrupt and reshape cell membranes, which may affect natural cell culture, growth, and proliferation.

To address these challenges, we demonstrate intracellular potential recording of cardiomyocytes using simple 2D planar electrode array in standard CMOS without any patch clamp or post fabrication of 3D nanoelectrode. This is enabled by our unique cardiomyocytes/fibroblasts co-culturing technique and cellular electroporation. The mixed co-culture with cardiac fibroblasts makes the cardiomyocytes to spread out on the chip surface and draws cardiomyocytes substantially closer to the electrodes, which significantly increases the sealing resistance. A local electrical pulse can be efficiently delivered to cells due to this tight cell sealing of electrode and successfully creates membrane poration with a low electrical pulse amplitude $\times$ duration threshold. This membrane poration drastically reduces the junctional membrane impedance, creates electrical access into cells, and enables high fidelity intracellular potential recording (Asphahani et al., 2007; Truskey et al., 1992).

In this paper, we first demonstrate the enhanced sealing resistance of cardiomyocytes with the increased fibroblast co-culture contents, proving that fibroblast co-culturing indeed promotes tight adhesion of cardiomyocytes on electrodes and results in high sealing resistance. Then, we characterize the membrane electroporation behaviours of cardiomyocytes for different electrical pulse conditions on the mixed co-cultures. Next, we present the recorded intracellular potential signals of two major types of cardiac cells: ventricular myocytes and induced pacemaker cells, both with high signal fidelity and accuracy. The recorded intracellular potential signals are further verified by administrations of various antiarrhythmic drugs, including lidocaine and verapamil. Compared to 3D nanoelectrodes and patch clamp techniques, the proposed intracellular potential recording scheme uses simple CMOS 2D microelectrode array without any complex post fabrication. Benefiting from standard CMOS processes, our technology has the potential to achieve following unique advantages: (i) high-density electrodes with cellular to sub-cellular resolution yet fully scalable to massively large array for tissue-level monitoring, (ii) individual addressability of each electrode, (iii) parallel recording of hundreds to thousands of electrodes, (iv) high yield and cost efficiency, and (v) using built-in underlying CMOS analog/digital circuits for low-noise on-chip signal processing and computation. With these advantages, our technology may pave the way toward fully-automated high-throughput cost-effective cell-based assay platform for drug screening and early stage drug development, as well as accelerating numerous experimental processes in biology and biotechnology research.

2. Materials and methods

2.1. The fully packaged CMOS quad-modal sensor/stimulator cellular interfacing array

The sensor array chip is implemented in a standard 130 nm CMOS process with a chip size of 2 mm $\times$ 3 mm and the sensing/stimulation area of 1.85 mm $\times$ 1.85 mm. The chip contains 1024 quad-modal pixels with an individual pixel size of 58μm $\times$ 58 μm. Each quad-modal pixel supports intra/extra-cellular potential recording, complex cellular impedance measurement, optical recording, and biphasic current stimulation. For biocompatible interface, CMOS foundry default aluminium electrodes are modified to gold by following an in-house electroless gold plating process. The chip is mounted on a printed circuit board (PCB) and on-board packaged with biocompatible materials including medical epoxy, gold bond wires, and Polydimethylsiloxane (PDMS). The operation details of the CMOS chip, the electrode modification, and the biocompatible packaging are explained in the paper (Park et al., 2016, 2018a).

2.2. Neonatal rat ventricular myocytes and fibroblasts isolation

Neonatal rat ventricular myocytes (NRVMs) and cardiac fibroblast were enzymatically isolated from 1 to 2 days old neonatal rat pups and cultured as monolayers as previously described (Kapoor et al., 2011, 2013). NVRMs were transduced with an Ad-GFP vector (MOI of 1) for 2 h at RT in suspension. Similarly, induced pacemaker (iPM) cells were created via transduction of NRVMs with Ad-CMV-TBX18-IRES-ZsGReen1 (MOI = 1) 2 h at RT in suspension. Both NRVMs and iPM cells are fluorescent under fluorescent microscope.

2.3. The mixed spheroids formation with different contents of fibroblasts

Following transduction in suspension, cells were spun down and washed once with Dulbecco's Phosphate-Buffered Saline (DPBS). After washing, spheroids were formed using AggreWell™ (STEMCELL, Vancouver, Canada) as previously described (Kapoor et al., 2011, 2013). Cells were seeded to create spheroids of approximately 1000 cells/sphere. For spheroids with higher percentages of cardiac fibroblasts, the same number of cells per spheroids was maintained at 1000 cells/sphere, with reduced number of NRVMs/iPM cells to accommodate the increased contents of the fibroblasts. The mixing ratio and/or the fibroblast contest is defined as N (fibroblasts)/{N (fibroblasts) + N (cardiomyocytes)} $\times$ 100% where N () indicates the number of specific cells. Experiments with murine subjects were performed in compliance with the relevant laws and institutional guidelines and were approved by the IACUC of Emory University.

2.4. The on-chip cell transfer and cell culture

The packaged chip is washed with 70% ethanol and DPBS for 3 times. Fibronectin is coated to the surface of chip at a concentration of 50ug/mL and allowed to bind for 2 h at 37 °C. Just before addition of cells, fibronectin is removed and 500uL of 10% NRVM media is added in a dome shape onto the chip. Three days post spheroid formation, spheroids are displaced from individual AggreWell™ and filtered with 40 μm cell strainers (Corning, NY) to remove single cells. The spheroids are concentrated into 1.5 mL Eppendorf tubes and allowed to sink to the bottom. The concentrated spheroid pellets are carefully pipetted onto the chip surface under a stereoscope to visualize localization of

spheroids. The chip is unmoved for 30 min to allow spheroids to stick onto surface before they are moved into incubator for overnight attachment. The culture medium is refreshed per 2 days.

2.5. The measurement setup and electrophysiology recording

The cell-loaded packaged PCB module is completely covered by a custom designed Faraday metal cage for electromagnetic shielding and D type battery is used for power supply to remove 60Hz noise. The chip is configured through a digital serial-to-parallel interface at a clock frequency of 2 MHz and the chip output data is acquired and stored in personal computer memory by FPGA (USB1616HS). The chip is programmed by LabVIEW (National Instrument) and the measured data is processed in MATLAB (MathWorks). For electrophysiology measurements, after the mixed spheroids are pipetted to the chip, we incubate the cell-loaded packaged PCB module for 24 h to allow initial cell attachment to the surface. After 24 h of incubation, the impedance measurements are performed and after 48 h of incubation, potential recordings are performed.

3. Results and discussion

3.1. Proliferation and migration of cells and the cell-electrode sealing resistance

Cell adhesion on in vitro cultured surface is a fundamental physiological process that involves changes in cell morphology and cytoskeletal structures and regulates cell migration and tissue development (Asphahani et al., 2007; Truskey et al., 1992; Zitzmann et al., 2017; Um et al., 2017). Cellular adhesion, including spreading, immobilization, attachment, migration, and proliferation, is often characterized by electrical cellular impedance measurement using individually addressable electrode arrays. Fig. 1a shows an equivalent circuit model of the cell-to-electrode interface impedance (Asphahani et al., 2007). For the cellular impedance measurement, two adjacent electrodes sealed by the cellular samples are selected: one for the driving voltage ($V_{ex.}$) and the other for measuring the resultant current ($I_{sens.}$). Then, the complex cellular impedance, as the amplitude and phase values of the ratio of $V_{ex.}/I_{sens.}$, is obtained (Fig. S1). The cell-to-electrode interface, including the culture medium, can be electrically modelled by the electrode-electrolyte impedance (Z_e), the junctional membrane impedance (Z_j), the solution resistance ($R_{solution}$), and the sealing resistance (R_{seal}) (Spira et al., 2013). The junctional membrane impedance and the sealing resistance are of particular importance. The junctional membrane impedance, i.e., the cell membrane impedance, is modelled by a resistor in parallel with a capacitor (C_m). It behaves as an electrical insulator (C_m) that hinders intracellular potential monitoring using conventional extracellular electrodes. Thus, for intracellular potential monitoring, a low junctional membrane impedance is desired, which can be achieved by membrane poration. On the other hand, the sealing resistance is the leakage current path resistance (I_{sol} in Fig. 1a) due to a very thin solution layer formed between the electrode and cell membrane, e.g., typically with a thickness of 10 nm–15nm (sealing gap thickness in Fig. 1a) (Asphahani et al., 2007; Truskey et al., 1992). It represents how tightly the electrodes are sealed by cells. A smaller sealing gap results in a higher sealing resistance and tighter sealing, which minimizes the leakage current path and is desired for both cellular potential recording and electroporation. During the potential recording, the ion-channel current to voltage conversion efficiency increases with R_{seal}, resulting in an increased signal-to-noise ratio (Spira et al., 2013). For electroporation, with higher R_{seal}, the electrical pulses can be more efficiently delivered to the cell membranes, allowing the use of pulses with lower voltages for improved safety. The increased sealing resistance can be manifested as the phase of the measured

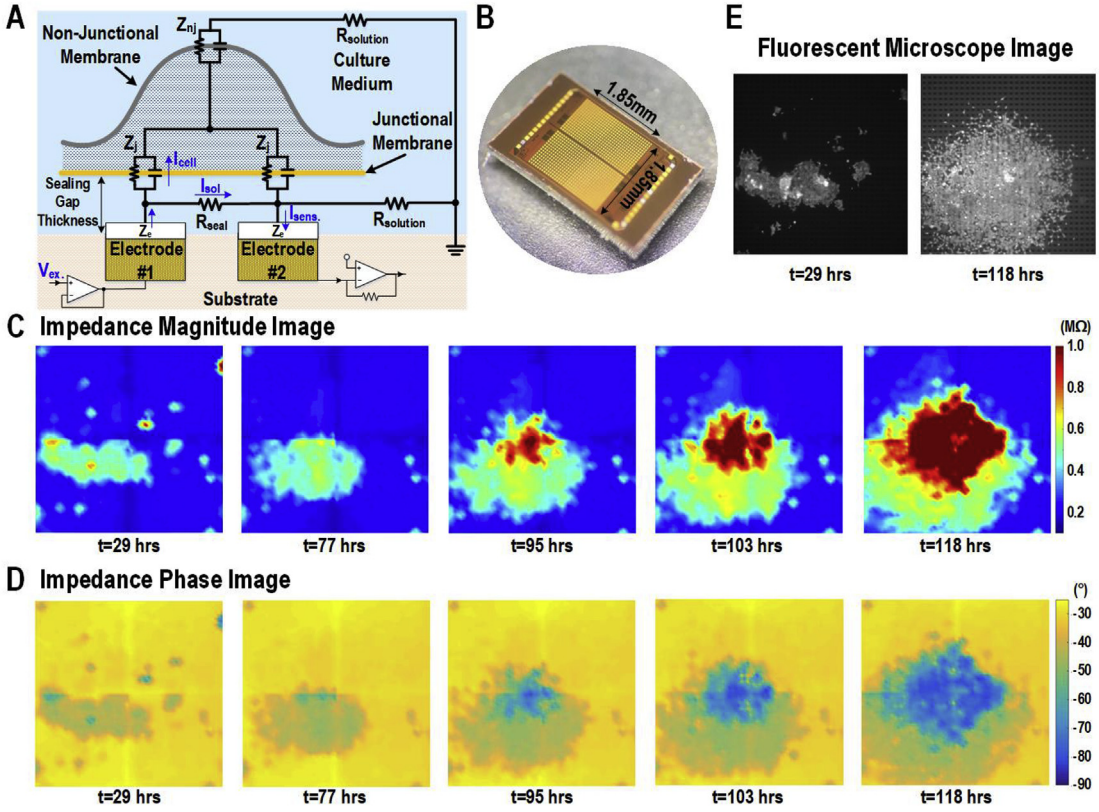

Fig. 1. The time-lapse impedance measurement of HEK cell with CMOS quad-modal cellular interfacing chip. (**A**) The equivalent electrical circuit model of the cell-to-electrode interface impedance. (**B**) The CMOS quad-modal cellular interfacing array chip (Park et al., 2016, 2018a; 2018b). (**C** and **D**) The time-lapse measured HEK cell impedance (C) magnitude images and (D) phase images at 100 kHz. (**E**) The reference fluorescent microscope image of HEK cell.

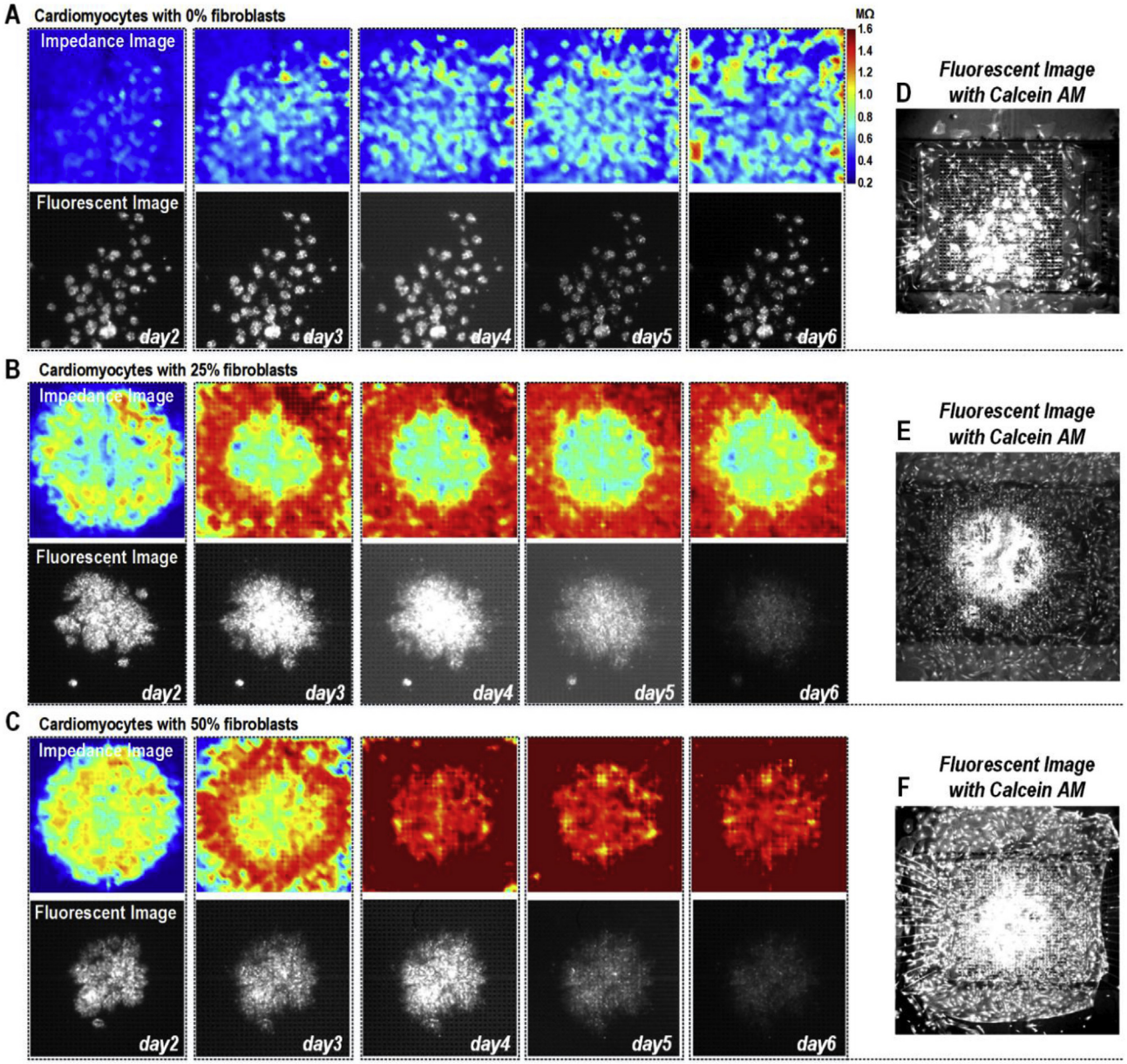

Fig. 2. The time-lapse measured impedance magnitude images of the mixed spheroids with different fibroblasts contents. (**A**, **B**, and **C**) The impedance magnitude images of the mixed spheroids with (A) 0%, (B) 25%, and (C) 50% fibroblasts contents each with the reference fluorescent microscope images. (**D**, **E**, and **F**) The reference fluorescent microscope images of the mixed spheroids with the fibroblast contents of (D) 0%, (E) 25%, and (F) 50% with the addition of Calcein AM to visualize cardiomyocytes as well as non-myocytes cells. Note that the fluorescent microscope images can only visualize the cardiomyocytes without the addition of Calcein AM. The Calcein AM is added at the end of the experiments and can visualize most of the eukaryotic cells. All figures share the same impedance scale bar.

complex impedance $\{\angle(R_{seal}//1/sC_m) = \tan^{-1}(-\omega_0 R_{seal} C_m)$, where $s = j\omega_0$ and ω_0 = angular frequency$\}$ changes 0° to −90° and at the same time, the magnitude of the measured complex impedance $\{|R_{seal}//1/sC_m| = R_{seal}/\sqrt{(1+\omega_0^2 R_{seal}^2 C_m^2)}\}$ increases.

In this section, we will present the relation between the sealing resistance and the cell proliferation. It has been shown (Baumann et al., 1997; Asphahani et al., 2007; Giaever et al., 1993; Huang et al., 2004; Lehnert et al., 2003; Truskey et al., 1992) that as cells proliferate and spread into the empty area, the sealing gap thickness between the cell and culture surface decreases. This cellular behaviour is also observed and verified by cellular impedance measurements using our CMOS quad-modal cellular interfacing array chip. In this experiment, human embryonic kidney cells (HEK-293) are cultured in vitro on the CMOS chip surface. HEK cells cannot grow as a multilayer due to a contact inhibition of growth (Leontieva et al., 2014; Ribatti et al., 2017). When these cells reach 100% density, biological processes begin to inhibit proliferation. The HEK cells are clustered in one area because they are grown as small spheroids aggregates and then allowed to attach/spread onto the substrate surface. The time-lapse cellular impedance measurements are performed at the frequency of 100 kHz and the measured time-lapse cellular impedance magnitude and phase are shown in Fig. 1c and d, respectively, with the reference fluorescent microscope images taken at t = 29 h and t = 118 h (Fig. 1e). The impedance images reveal that as HEK cells proliferate and spread into empty chip area, the sealing resistance increases. After 95 h, HEK cells achieve a close contact to the CMOS chip surface at the centre, shown as a large measured impedance magnitude (Fig. 1c), and such closely contacted area expands over time due to the cell spreading and proliferation, which is consistent with the reported results (Asphahani et al., 2007; Truskey et al., 1992). The time-lapse phase of the cellular impedance is shown in

Fig. 1d, revealing different but equally important information. As the sealing resistance (R_{seal}) increases, the leakage current (I_{sol}) through the thin cell-chip gap decreases, while the current through the cell-membrane (I_{cell}) increases. This current is capacitively coupled into cells, resulting in a more capacitive cellular impedance, i.e., impedance phase approaching -90°. The time-lapse cellular impedance measurements with both magnitude and phase (Fig. 1c and d) well match the aforementioned observations, further verifying the relation between the cell proliferation and cell-chip sealing and adhesion.

3.2. Sealing resistance of cardiomyocytes mixed co-culture with the cardiac fibroblasts

To measure the intracellular action potential of cardiomyocytes using only 2D electrodes, tight sealing between cells and electrodes is critical. However, unlike HEK cells, cardiomyocytes only slightly spread on culture surface and do not proliferate during in vitro culture, which often results in their loose surface attachment and low sealing resistance. Consequently, electroporation on in vitro cultured cardiomyocytes typically requires high electrical pulses that exceed the safety range of the electrodes, making 2D planar electrodes unsuitable for intracellular potentials recording. On the other hand, in vitro cultured cardiac fibroblasts are known to rapidly proliferate and expand on culture surface together with secretion of gel-like enriched extracellular matrix for surface adhesion enhancement, leading to a reduced sealing gap thickness with a high sealing resistance (Camelliti et al., 2005). Furthermore, cardiac fibroblasts are electrically non-excitable, do not experience cardiac action potential process, and do not generate action potential signals. Therefore, the following measured intracellular action potential signals are from cardiomyocytes.

In this paper, we hypothesize that mixed co-culture of cardiac fibroblasts and cardiomyocytes establishes tight adhesion of the latter to the chip surface and electrodes, which then enables high-fidelity intracellular potential monitoring of cardiomyocytes by electroporation using only 2D planar electrodes. The following experiments are performed to test this hypothesis. Cardiomyocytes are uniformly mixed with cardiac fibroblasts as mixed spheroids with average diameter of 100 μm using AggreWell™. The mixed spheroids are pipetted to the fibronectin coated CMOS quad-modal cellular interfacing array chip. Based on mixed cardiomyocytes/fibroblasts spheroids with approximate fibroblasts contents of 0%, 25%, and 50%, we perform time-lapse cellular impedance measurements, shown in Fig. 2a, b, and 2c, respectively. Note that a small volume of other non-myocyte cells including endothelial cells, macrophages, and smooth muscle cells are included in the mixed spheroids, while only cardiomyocytes are fluorescent without addition of Calcein AM due to the reporters added by the viruses, revealing themselves amongst fibroblasts and the other non-myocyte cells in the fluorescent images. Eventually, we add Calcein AM at the end of the experiment to visualize other cell types in the final reference fluorescent images shown in Fig. 2d, e, and 2f.

First, the measured cellular impedance magnitude images of cardiomyocytes spheroids with approximately 0% fibroblasts are shown in Fig. 2a. The spheroids start to adhere to the sensor surface on day 2 (Fig. 2a) and the sealing resistance gradually increases over time and then saturates. After day 4, we observe that non-myocyte cells proliferate and migrate, which are eventually visualized by the reference fluorescent image (Fig. 2d) with Calcein AM addition. Note that as the measurement baseline, the culture medium impedance without any cells is measured over 11 days with an average impedance magnitude of 0.217MΩ (Fig. S2). Next, the mixed spheroids with 25% fibroblast contents are pipetted onto the chip, and the measured impedance magnitude images together with the reference fluorescent images over 6 days are shown in Fig. 2b. Unlike cardiomyocytes spheroids with approximately 0% fibroblast content (Fig. 2a), most mixed spheroids are connected together as tissues at the centre area of the chip on day 2 shown in the fluorescent image (Fig. 2b). The impedance magnitude image on day 2 shows that the peripheral area presents a higher impedance than the centre area. This is because the fibroblasts rapidly proliferate and migrate out to the peripheral area (Fig. S3). After day 3, fibroblasts further proliferate, migrate out to the empty sensor area, and achieve a full confluence, which is confirmed by the fluorescent image with Calcein AM addition (Fig. 2e). The mixed spheroids at the centre also expand and spread over time with higher sealing resistance than the cardiomyocytes-only spheroids. Lastly, the mixed spheroids with the fibroblasts content of 50% are pipetted to the chip and the measured impedance magnitude images are shown in Fig. 2c. The time-lapse impedance magnitude images show that the fibroblasts proliferate and migrate out to the empty peripheral area and the sealing resistance of the peripheral area increases over time. The mixed spheroids are connected as a tissue at the centre of the chip. The mixed spheroids with 50% fibroblast content present a higher sealing resistance than the mixed spheroids with 0%/25% fibroblast content.

These experiments verify that the mixed spheroids with higher fibroblast contents establish tight sealing between cells and chip surface/electrodes. This cellular property is then shown to enable intracellular potential recording via electroporation using only 2D planar electrodes. After the experiments, the cultured cells are trypsinized and washed, and then the electrode-electrolyte interfacial impedance is then measured, whose results are close to the measured electro-electrolyte impedance before seeding the cells (Fig. S2). These additional measurements verify that the electrodes were electrochemically stable and intact during the experiments and validate the cellular impedance measurements.

3.3. Intracellular potential measurement by electroporation using 2D planar electrodes

In this section, we will present the intracellular action potential measurement by electroporation using only 2D electrodes on in vitro cultured mixed cardiomyocyte/fibroblast spheroids. The fibroblasts content is 40% in the mixed spheroids to promote tight surface affinity attachment of cardiomyocytes. We first investigate the relationship among three major parameters of electroporation pulses (pulse amplitude, duration, and number of pulse trains), the resultant membrane poration, and intracellular potential signals. Then, we will show the intracellular potential signal fidelity. The measured intracellular potential signals of two types of well-characterized cardiomyocytes are presented to check the validity of the measurements and signal fidelity.

Mixed spheroids with 40% fibroblasts content are pipetted onto the CMOS chip, which connect together and form a synchronized tissue after day 2. Next, the electroporation and intracellular potential recording are sequentially performed with the details explained as follows (Fig. 3a). First, to electroporate the target cell membrane at a specific location on the CMOS chip, two adjacent electrodes sealed by the tissue are selected; one for the current excitation and the other for the reference. Then, a train of electrical pulses is delivered to the selected current excitation electrode. After the electrical pulses, the same electrode selected for the current excitation is connected to the potential recording amplifier on the CMOS chip to record the electrode's nearby local cellular potential. During the cellular potential recording, an additional pair of electrodes at the edge of the synchronized tissue are selected to pace the cells. We select the two pacing electrodes with sufficient distance from the potential recording site to minimize the stimulation artiefacts. In summary, we first perform electroporation using a pair of adjacent electrodes both sealed by the synchronized tissue. After the electroporation, we monitor the local potentials at the same location where the nanopores in the cell membrane are created. In addition, we control the initiation of the action potentials of the synchronized tissue with concurrent pacing stimulations to precisely regulate the cell's beating frequency.

The measured local potentials after electroporation with different pulse parameters (amplitude, duration, and total number of pulses in

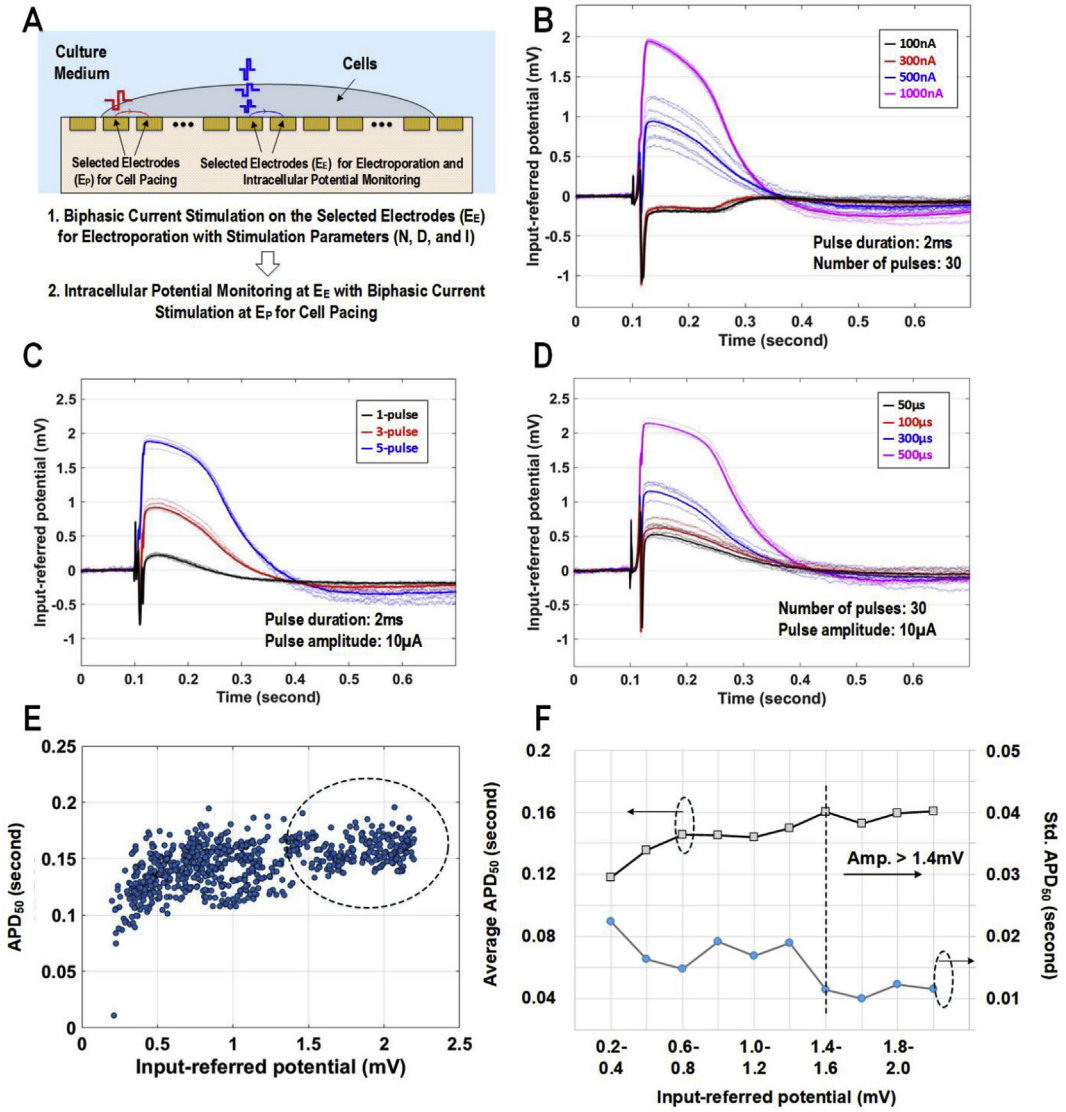

Fig. 3. Characterization of the membrane electroporation behaviours of cardiomyocytes for different electrical pulse conditions. (**A**) The sequence of the intracellular potential signal measurements. (**B**, **C**, and **D**) The measured potential signals after electrical pulses each with different (B) pulse amplitude, (C) number of pulses, and (D) pulse duration, while the other parameters are fixed. (**E**) The extracted action potential durations at 50% repolarization (APD_{50}) versus the input-referred potential amplitudes based on 762 measured potential signals. (**F**) The statistical summary of the measured data in (E). The average (square) and the standard deviation (circle) of the extracted APD_{50}s per each intracellular potential signal amplitude interval (ranging from 0.2 mV to 2.2 mV with the step of 0.2 mV) are summarized.

the pulse train) are shown in Fig. 3. To characterize the effect of each pulse parameter on the electroporation of the cell membrane, we vary one pulse parameter while the other two parameters are fixed. In Fig. 3b, as the current pulse amplitude increases from 100 nA to 1 μA with a fixed 30 pulses in the pulse train and 2 ms duration for each pulse, the recorded intracellular potentials signal amplitude increases, indicating that the junctional membrane impedance (Z_j) decreases with more nanopores created in the membrane. Similarly, as the number of pulses or pulse duration increase, more nanopores are formed through electroporation, and the recorded intracellular potential signal amplitude increases as well (Fig. 3c and d). Thus, we identify and verify three electrical pulse parameters that can be used to control the formation of membrane nanopores during electroporation, which modulate the local junctional membrane impedance and enable successful intracellular potential recording using only 2D electrodes.

We further elaborate on the fact that low junctional membrane impedance after electroporation is essential for reliable monitoring of intracellular potential signals. Here, we will show the effect of the intracellular potential signal amplitude on the fidelity of action potential signal parameters. In this experiment, 762 measurement samples of cellular potential signals are investigated with different electroporation pulse strength and a wide range of junctional membrane impedances after electroporation. To evaluate the recorded signal fidelity, the input-referred intracellular potential amplitude and action potential duration at 50% repolarization (APD_{50}) are extracted from the 762 cellular potential measurements and summarized in Fig. 3e and f. The results reveal that as the measured potential signal increases, the average APD_{50} increases and then stabilizes at around 160 ms after the potential signal amplitudes exceed 1.4 mV. Furthermore, as the potential signal amplitude increases, the standard deviation of APD_{50} reduces as well, indicating that a high signal fidelity is achieved for the cellular signal feature extractions with the potential amplitude > 1.4 mV. For the experiments in the following section, to ensure high signal fidelity, we use recorded intracellular potential signals with an amplitude > 1.4 mV. With our current 28μm × 28 μm electrode, a local electrical pulse could create membrane poration on multiple cells whose

membranes are directly interfaced with the electrode and the intracellular potential signals combined from multiple cells could be measured. However, since cardiomyocytes are coupled together and synchronized, the intracellular potential signals from multiple cells attached to the electrode within 28μm × 28 μm are coherent and in-phase combined without signal distortions. Although the intracellular potential amplitude could potentially change with the number of cells, the intracellular action potential shape maintains same, which shows full cardiac action potential phases and contains essential physiological information for drug screening.

3.4. The intracellular potential recordings of ventricular myocytes and induced pacemaker cells with antiarrhythmic drugs administrations

The intracellular potentials of two distinct types of cardiac cells, i.e., ventricular myocytes and pacemaker cells, are measured to further verify our method and the resultant signal fidelity. The idea is to examine two populations of cardiac cells that are discernible by their unique action potential morphologies: pacemaker cells express high funny current I_f, which allows for spontaneous and autonomous beating (Brown et al., 1979) and low inward rectifier current I_{K1} (Brown and Difrancesco, 1980), while ventricular myocytes express dependence of voltage gated Na^+ channels to depolarize (Saint et al., 1992) and high I_{K1} (Wang et al., 1998) to prevent unwanted spontaneous activation (Dhamoon and Jalife, 2005). To this end, freshly-isolated and cultured neonatal rat ventricular myocytes (NRVMs) are employed as one of the most extensively-characterized model of primary ventricular cardiomyocytes (Harary and Farley, 1963). We exploit our genetically engineered pacemaker cell platform, created by reprogramming NRVMs with an embryonic single transcription factor, Tbx18 (Kapoor et al., 2011, 2013; Hu et al., 2014). These induced pacemaker (iPM) cells exhibit hallmarks of cardiac pacemaker cells such as HCN4 ion channels, which encodes the funny current I_f (Altomare et al., 2003). I_f begins at phase 4 of the pacemaker action potential with a slow inward flow of K^+ and Na^+ followed by L-type and T-type calcium currents that dominate the potential upstroke seen in phase 0. Noting that non-myocytes such as fibroblasts account for a significant number of myocardial cells (Camelliti et al., 2005; Pinto et al., 2016) and to enhance attachment of cardiac myocytes on the CMOS chip surface, NRVMs and iPM cells are mixed with cardiac fibroblasts to form spheroids consisting of 60% cardiomyocytes (either NRVMs or iPM cells) and 40% fibroblasts. Fig. 4a and b shows the input-referred intracellular potential signals of NRVMs and iPM cells measured at 5 different locations, i.e., sensor pixels, on the CMOS chip. After electroporation, intracellular potentials are recorded with the concurrent cell pacing at 1Hz in order to mitigate beating rate-dependent adaptation of action potential duration in cardiac myocytes (Ronaldson-Bouchard et al., 2018). Note that for the following experiments, we pace cells to regulate beating rate. The measured input-referred intracellular potential signal amplitude is greater than 1.4 mV for both NRVMs and iPM cells, and the intracellular potential signals measured at five different sensor pixels achieve a high signal-to-noise ratio with a pacing capture rate of 100%. Capture rate is defined as the number of synchronized beatings upon stimulations divided by the number of stimulation pulses. Next, the measured intracellular potentials of NRVMs and iPM cells are superimposed for comparison with the average waveforms highlighted (Fig. 4c). The recorded signals clearly show that iPM cells exhibit a slower phase 0 upstroke velocity and a shorter action potential duration compared to the NRVMs, which are consistent with reported results (Kapoor et al., 2011, 2013). Fig. 4d summarizes the extracted upstroke velocity and action potential duration at 50% repolarization (APD_{50}) of iPM cells and NRVMs. The NRVMs and iPM cells are clearly distinguishable as two clusters based on upstroke velocity (dv/dt) and action potential duration (APD_{50}), which match the distinctive cellular properties of NRVMs and iPM cells well and verify the accuracy and the fidelity of the measured intracellular potential signals (Kapoor et al., 2011, 2013). We then ask how long intracellular potential monitoring could be performed reliably. After electroporation, highly consistent intracellular potential signals are recorded > 300 s as shown in Fig. 4e. The measured average intracellular potential signal amplitude is 4 mV right after electroporation, and then gradually decreased, presumably due to the membrane resealing. Nonetheless, the shape of intracellular action potential signal is maintained throughout the recording period. The statistical summary (Fig. 4e) and the time overlay plot (Fig. 4f) indicate that APD_{50} measurements are consistent, highlighting the reliability of long-term measurements.

Intracellular action potentials and rhythmic contractility of cardiac myocytes are indispensable for gauging efficacy and toxicity during drug discovery pipeline (Aiba et al., 2005; Bedut et al., 2016; Chen et al., 2013; Gibson et al., 2014; Hensley et al., 1997; Peng et al., 2010; Wang et al., 2012; Zhang et al., 1999). We ask if intracellular action potential measurements on the CMOS chip could recapitulate the predicted effects of ion channel drugs with known modes of action. Lidocaine is a specific blocker of voltage-gated Na^+ channels (Sheets and Hanck, 2003). Na^+ channels exhibit fast gating mechanisms and dominate the early depolarizing phase of an action potential in ventricular myocytes (Saint et al., 1992). Application of lidocaine decreases the maximum upstroke velocity of NRVMs in a dose-dependent manner (Fig. 5a and b). Blockade of inward Na^+ current with lidocaine decreases action potential duration at 80% repolarization (APD_{80}) as well (Fig. 5a and b), in line with the known effects of lidocaine on cardiac myocytes' action potential upstroke velocity and duration (Josephson et al., 1988). Plotting action potential upstroke velocities against APD_{80} in a 2-dimensional plot accentuate the dose-dependent nature of Na^+ channel inhibition by lidocaine (Fig. 5c), which are routine parameters to examine for propensity to cardiac arrhythmias. Next, we measure intracellular potential signals of iPM cells upon application of 300 nM verapamil (Fig. 5d). Verapamil is a class-IV antiarrhythmic and a blocker of L-type Ca^{2+} channels (Cranefield et al., 1974). L-type Ca^{2+} channels open as Na^+ channels become inactivated, and contribute to prolongation of AP duration. As anticipated, APD_{80} and APD_{50} of iPM cells became significantly reduced upon application of 300 nM verapamil (Fig. 5e and f). This further verifies the fidelity of the intracellular action potential measurements on our CMOS chip. Taken together, these measurements demonstrate the high signal fidelity and utility of our platform for high throughput drug screen at the early stage of new drug development (Drews, 2000; Feng et al., 2009; Scannell et al., 2012; Gintant et al., 2016; Park et al., 2016, 2018a, 2018b).

4. Conclusion

We propose and demonstrate intracellular action potential recording of cardiomyocytes only using 2D planar electrode array provided by a standard low-cost CMOS process without using patch clamps or any post-fabricated vertical 3D nanoelectrodes. We use fibroblasts co-culturing and electroporation techniques to monitor intracellular action potential of cardiomyocytes with high signal fidelity. For demonstration, we use a CMOS 1024-pixel quad-modal cellular interfacing array chip that is capable of cellular impedance measurement, intra/extra-cellular potential recording, optical recording, and stimulation (Park et al., 2016, 2018a; 2018b). We observe that many in vitro cultured cells with proliferation and migration properties such as fibroblasts and HEK cells exhibit remarkably tight adhesion with culture surface/electrode, which is manifested as their high sealing impedance. Then we propose to mix cardiomyocytes and cardiac fibroblasts as spheroids and co-culture them to enhance the surface adhesion of cardiomyocytes. This approach successfully achieves high-fidelity intracellular potential monitoring of cardiomyocytes by electroporation only using 2D planar electrodes. Note that our unique multi-modal cellular interfacing chip allows us to characterize cell-to-surface adhesion, perform electroporation, and record intracellular potential signals. Our proposed techniques do not require any patch clamp or post-

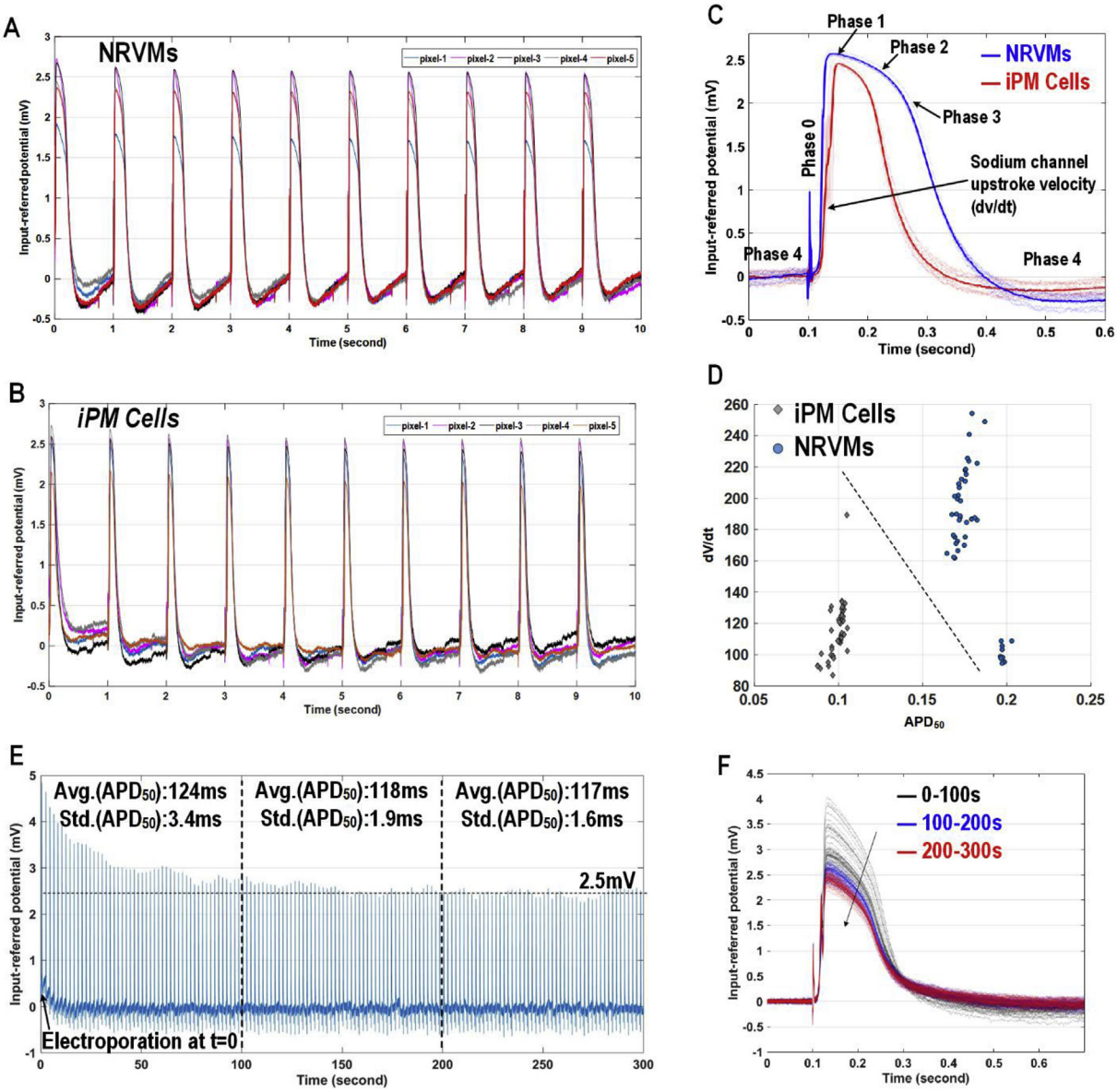

Fig. 4. Intracellular potential recording of two distinct types of cardiac cells. (**A** and **B**) The intracellular potential signals of (A) NRVMs and (B) iPM cells measured at 5 different pixels with the concurrent cell pacing at 1Hz. (**C**) The overlay plot of the intracellular potential signals of NRVMs and iPM cells with the average line highlighted. (**D**) The summary of the extracted APD_{50} and the phase 0 upstroke velocity of NRVMs and iPM cells. (**E**) The long-term transient intracellular potential signals. (**F**) The time overlay plot of the intracellular potential signals of iPM cells recorded for 300 s.

fabricated vertical 3D nanoelectrodes, and can be directly implemented in highly scaled CMOS processes, e.g., 7 nm CMOS, to achieve substantial pixel size reduction and array size increase in the future. Therefore, it can be readily scaled to an ultra-high density and an ultra-high throughput cellular sensor/actuator array with sub-cellular resolution, tissue level field of view, high yield, and low cost.

In this paper, we verify the relationship between cell proliferation/migration and the cell-surface sealing resistance based on HEK cells using a CMOS quad-modal sensor chip. The measured time-lapse impedance magnitude/phase images show that as HEK cells proliferate and migrate, the cells tightly seal the culture surface and electrodes. Next, we uniformly mix cardiomyocytes with cardiac fibroblasts as spheroids for different fibroblasts contents and then characterize the proliferation and surface adherence of the mixed spheroids using time-lapse impedance measurements. The measured impedance shows that mixtures with high fibroblast contents exhibit high sealing resistance and strong adherence, which enables tight attachment of cardiomyocytes on electrodes and culture surface, successful electroporation, and intracellular potential recording of cardiomyocytes only using 2D planar electrodes with low electroporation pulse strength. Furthermore, we characterize and identify three major electrical pulse parameters that determine the success of electroporation. In addition, intracellular potential signal fidelity and accuracy are verified through extensive cell-based measurements. The intracellular potential signals of NRVMs and iPM cardiac cells are measured based on the mixed spheroid technique with cardiac fibroblasts, and key cellular action potential parameters such as the action potential duration and phase 0 upstroke velocity are extracted. The distinct cellular characteristics of NRVMs and iPM cells are accurately captured, verifying high fidelity of the intracellular potential signals measured by our 2D planar electrode array. Finally, the intracellular potential signals of NRVMs and iPM cells are measured with the administration of antiarrhythmic drugs of lidocaine and verapamil at different concentrations. The measured intracellular potential signals and the extracted cellular parameters reliably capture the drugs dose-dependent cellular responses, which match well with the known drug effects and verify the use of our

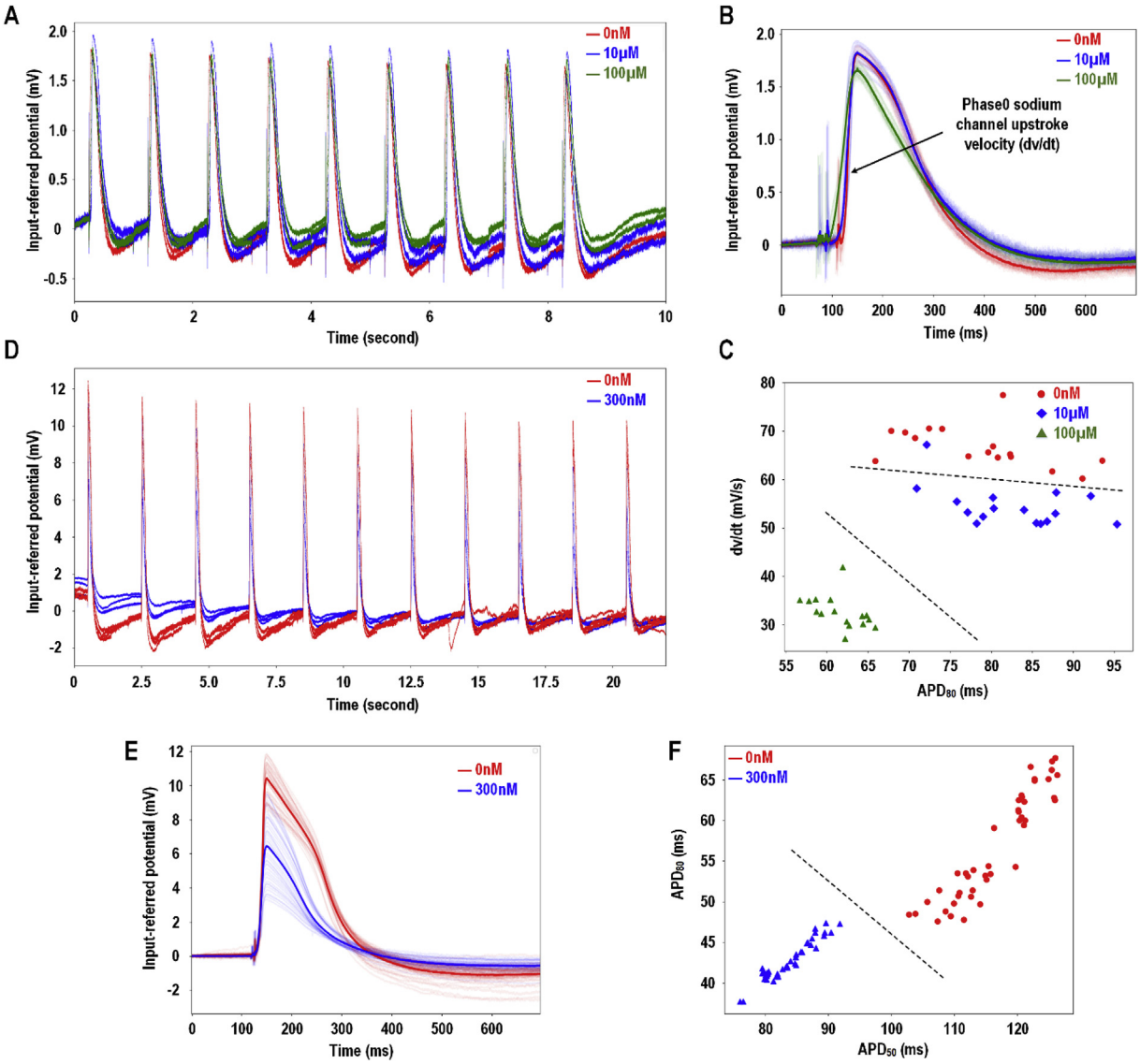

Fig. 5. Intracellular potential recording with the administration of antiarrhythmic drugs. (**A**) The measured transient intracellular potentials of NRVMs with lidocaine administration. (**B**) The overlay plots of the intracellular potentials each with lidocaine concentration of 0 nM, 10 μM, and 100 μM. (**C**) The summary of the extracted phase 0 upstroke velocities (dv/dt) and ADP_{80} of NRVMs each with different lidocaine concentration. (**D**) The measured transient intracellular potentials of iPM cells with verapamil administration. (**E**) The overlay plots of the intracellular potentials each with verapamil concentration of 0 nM and 300 nM. (**F**) The summary of the extracted APD_{50} and ADP_{80} of iPM cells each with different verapamil concentration.

platform for high throughput drug screening and new drug development. As future work, it will be highly beneficial to further increase the number of pixels and parallel recording/stimulation channels, as well as the spatiotemporal resolutions (pixel pitch), for a single-cell resolution sensing/actuation. Furthermore, in order to precisely select/monitor a target single cell, various single-cell patterning techniques such as 3D/inkjet printings and integrin-mediated cell patterning can be investigated on CMOS surface. Other cellular sensing modalities, such as intracellular pH detection, may be added at the pixel level to further expand our capabilities of cell monitoring. Machine learning algorithm and computation hardware may be employed to facilitate cellular or physiological feature extraction and drug-dose dependent pattern recognition. Our mixed co-culture techniques and intracellular potential recording method using simple 2D electrodes may be extended to other electrogenic cells such as neurons.

Funding

The study was supported by NSF CAREER (1454555), NHLBI (1R01HL111646-01A1), NHLBI (5F31HL137367-02), and NSF (1609831).

Data and materials availability

All data needed to evaluate the conclusions in the paper are present in the paper and/or the supplementary materials. They can be obtained by contacting the authors. Additional data related to this paper may be requested from the authors.

CRediT authorship contribution statement

Jong Seok Park: Conceptualization, Software, Writing - original draft. **Sandra I. Grijalva:** Conceptualization, Writing - original draft. **Doohwan Jung:** Resources. **Sensen Li:** Resources. **Gregory V. Junek:** Writing - review & editing. **Taiyun Chi:** Conceptualization. **Hee Cheol Cho:** Conceptualization, Writing - original draft. **Hua Wang:** Conceptualization, Writing - original draft.

Declaration of competing interest

The authors declare that they have no known competing financial interests or personal relationships that could have appeared to influence the work reported in this paper.

Acknowledgments

General: We are grateful to the members of Georgia Electronics and MicroSystem (GEMS) Lab of Georgia Tech and Heart Regeneration Lab of Emory University for technical discussions.

Appendix A. Supplementary data

Supplementary data to this article can be found online at https://doi.org/10.1016/j.bios.2019.111626.

References

Abbott, J., Ye, T., Qin, L., Jorgolli, M., Gertner, R., Ham, D., Park, H., 2017. CMOS nanoelectrode array for all-electrical intracellular electrophysiological imaging. Nat. Nanotechnol. 12, 460–466.
Aiba, T., Shimizu, W., Inagaki, M., Noda, T., Miyoshi, S., Ding, W., Zankov, D., Toyoda, F., Matsuura, H., Horie, M., Sunagawa, K., 2005. Cellular and ionic mechanism for drug-induced long QT syndrome and effectiveness of verapamil. J. Am. Coll. Cardiol. 45, 300–307.
Altomare, C., Terragni, B., Brioschi, C., Milanesi, R., Pagliuca, C., Viscomi, C., Moroni, A., Baruscotti, M., DiFrancesco, D., 2003. Heteromeric HCN1-HCN4 channels: a comparison with native pacemaker channels from the rabbit sinoatrial node. J. Physiol. 549, 347–359.
Asphahani, F., Zhang, M., 2007. Cellular impedance biosensors for drug screening and toxin detection. Analyst 132, 835–841.
Baumann, R., Brischwein, M., Schwinde, A., Stegbauer, K., Wolf, B., 1997. Monitoring of cellular behaviour by impedance measurements on interdigitated electrode structures. Biosens. Bioelectron. 12, 29–41.
Bedut, S., Seminatore-Nole, C., Lamamy, V., Caignard, S., Boutin, J., Nosjean, O., Stephan, J., Coge, F., 2016. High-throughput drug profiling with voltage- and calcium-sensitive fluorescent probes in human iPSC-derived cardiomyocytes. Am. J. Physiol. Heart Circ. Physiol. 311, 44–53.
Brown, H., Difrancesco, D., 1980. Voltage-clamp investigations of membrane currents underlying pace-maker activity in rabbit sino-atrial node. J. Physiol. 308, 331–351.
Brown, H., Difrancesco, D., Noble, S.J., 1979. How does adrenaline accelerate the heart? Nature 280, 235–236.
Camelliti, P., Borg, T., Kohl, P., 2005. Structural and functional characterisation of cardiac fibroblasts. Cardiovasc. Res. 65, 40–51.
Chen, H., Zhang, D., Chao, S., Ren, J., Xu, L., Jiang, X., Wang, S., 2013. Comparison of the effects of antiarrhythmic drugs flecainide and verapamil on fKv1.4ΔN channel currents in Xenopus oocytes. Acta Pharmacol. Sin. 34, 221–230.
Cranefield, P.F., Aronson, R.S., Wit, A.L., 1974. Effect of verapamil on the noraml action potential and on a calcium-dependent slow response of canine cardiac Purkinje fibers. Circ. Res. 34, 204–213.
Dhamoon, A.S., Jalife, J., 2005. The inward rectifier current (Ik1) controls cardiac excitability and is involved in arrhythmogenesis. Heart Rhythm 2, 316–324.
Dipalo, M., Amin, H., Lovato, L., Moia, F., Caprettini, V., Messina, G., Tantussi, F., Berdondini, L., Angelis, F., 2017. Intracellular and extracellular recording of spontaneous action potentials in mammalian neurons and cardiac cells with 3D plasmonic nanoelectrodes. Nano Lett. 17, 3932–3939.
Drews, J., 2000. Drug discovery: a historical perspective. Science 287, 1960–1964.
Duan, X., Gao, R., Xie, P., Cohen-Karni, T., Qing, Q., Choe, H., Tian, B., Jiang, X., Lieber, C., 2012. Intracellular recordings of action potentials by an extracellular nanoscale field-effect transistor. Nat. Nanotechnol. 7, 174–179.
Feng, Y., Mitchison, T., Bender, A., Young, D., Tallarico, J., 2009. Multi-parameter phenotypic profiling: using cellular effects to characterize small-molecule compounds. Nat. Rev. Drug Discov. 8, 567–578.
Giaever, I., Keese, C., 1993. A morphological biosensor for mammalian cells. Nature 366, 591–592.
Gibson, J., Yue, Y., Bronson, J., Palmer, C., Numann, R., 2014. Human stem cell-derived cardiomyocytes detect drug-mediated changes in action potentials and ion currents. J. Pharmacol. Toxicol. Methods 70, 255–267.
Gintant, G., Sager, P., Stockbridge, N., 2016. Evolution of strategies to improve preclinical cardiac safety testing. Nat. Rev. Drug Discov. 15, 457–471.
Hai, A., Shappir, J., Spira, M., 2010. In-cell recordings by extracellular microelectrodes. Nat. Methods 7, 200–202.
Harary, I., Farley, B., 1963. In vitro studies on single beating rat heart cells. I. Growth and organization. Exp. Cell Res. 29, 451–465.
Hensley, J., Billman, G., Johnson, J., Hohl, C., Altschuld, R., 1997. Effects of calcium channel antagonists on Ca2+ transients in rat and canine cardiomyocytes. J. Mol. Cell. Cardiol. 29, 1037–1043.
Hu, Y.F., Dawkins, J., Cho, H., Marban, E., Cingolani, E., 2014. Biological pacemaker created by minimally invasive somatic reprogramming in pigs with complete heart block. Sci. Transl. Med. 6, 245ra94.
Huang, X., Nguyen, D., Greve, D., Domach, M., 2004. Simulation of microelectrode impedance change due to cell growth. IEEE Sens. J. 4, 576–583.
Josephson, I.R., 1988. Lidocaine blocks Na, Ca and K currents of chick ventricular myocytes. J. Mol. Cell. Cardiol. 20, 593–604.
Kapoor, N., Galang, G., Marbin, E., Cho, H., 2011. Transcriptional suppression of connexin43 by TBX18 undermines cell-cell electrical coupling in postnatal cardiomyocytes. J. Biol. Chem. 286, 14073–14079.
Kapoor, N., Liang, W., Marban, E., Cho, H., 2013. Direct conversion of quiescent cardiomyocytes to pacemaker cells by expression of Tbx18. Nat. Biotechnol. 31, 54–62.
Lehnert, D., Wehrle-Haller, B., David, C., Weiland, U., Ballestrem, C., Imhof, B., Bastmeyer, M., 2003. Cell behaviour on micropatterned substrata: limits of extracellular matrix geometry for spreading and adhesion. J. Cell Sci. 117, 41–52.
Leontieva, O., Demidenko, Z., Blagosklonny, M., 2014. Contact inhibition and high cell density deactivate the mammalian target of rapamycin pathway, thus suppressing the senescence program. Proc. Natl. Acad. Sci. U. S. A 111, 8832–8837.
Lin, Z., Xie, C., Osakada, Y., Cui, Y., Cui, B., 2014. Iridium oxide nanotube electrodes for sensitive and prolonged intracellular measurement of action potentials. Nat. Commun. 5, 3206.
Park, J., Chi, T., Su, A., Zhu, C., Sung, J., Cho, H., Styczynski, M., Wang, H., 2016. A high-density CMOS multi-modality joint sensor/stimulator array with 1024 pixels for holistic real-time cellular characterization. In: IEEE Symposium on VLSI Circuits (VLSI-Circuits), 15-17 June 2016. IEEE, Honolulu, HI, USA. https://doi.org/10.1109/VLSIC.2016.7573469. 22 September 2016, ISBN: 978-1-5090-0635-9, INSPEC Accession Number: 16322137, Print on Demand(PoD) ISBN: 978-1-5090-0636-6.
Park, J., Aziz, M., Li, S., Chi, T., Grijalva, S., Sung, J., Cho, H., Wang, H., 2018a. 1024-Pixel CMOS multimodality joint cellular sensor/stimulator array for real-time holistic cellular characterization and cell-based drug screening. IEEE Trans. Biomed. Circuits Syst. 12, 80–94.
Park, J., Grijalva, S., Aziz, M., Chi, T., Li, S., Sayegh, M., Wang, A., Cho, H., Wang, H., 2018b. Multi-parametric cell profiling with a CMOS quadmodality cellular interfacing array for label-free fully automated drug screening. Lab Chip 18, 3037–3050.
Peng, S., Lacerda, A., Kirsch, G., Brown, A., Bruening-Wright, A., 2010. The action potential and comparative pharmacology of stem cell-derived human cardiomyocytes. J. Pharmacol. Toxicol. Methods 61, 277–286.
Pinto, A.R., LLinykh, A., Ivey, M., Kuwabara, J., D'Antoni, M., Debuque, R., Chandran, A., Wang, L., Arora, K., Rosenthal, N., Tallquist, M., 2016. Revisiting cardiac cellular composition. Circ. Res. 118, 400–409.
Ribatti, D., 2017. A revisited concept: contact inhibition of growth. From cell biology to malignancy. Exp. Cell Res. 359, 17–19.
Robinson, J., Jorgolli, M., Shalek, A., Yoon, M., Gertner, R., Park, H., 2012. Vertical nanowire electrode arrays as a scalable platform for intracellular interfacing to neuronal circuits. Nat. Nanotechnol. 7, 180–184.
Ronaldson-Bouchard, K., Ma, S., Yeager, K., Chen, T., Song, L., Sirabella, D., Morikawa, K., Teles, D., Yazawa, M., Vunjak-Novakovic, G., 2018. Advanced maturation of human cardiac tissue grown from pluripotent stem cells. Nature 556, 239–243.
Saint, D.A., Ju, Y.K., Gage, P.W., 1992. A persistent sodium current in rat ventricular myocytes. J. Physiol. 453, 219–231.
Sakmann, B., Neher, E., 1984. Patch clamp techniques for studying ionic channels in excitable membranes. Annu. Rev. Physiol. 46, 455–472.
Sakmann, B., Neher, E., 2009. Single-Channel Recording, second ed. Springer.
Scannell, J., Blanckley, A., Boldon, H., Warrington, B., 2012. Diagnosing the decline in pharmaceutical R&D efficiency. Nat. Rev. Drug Discov. 11, 191–200.
Shalek, A.K., Robinson, J., Karp, E., Lee, J., Ahn, D., Yoon, M., Sutton, A., Jorgolli, M., Gertner, R., Gujral, T., MacBeath, G., Yang, E., Park, H., 2010. Vertical silicon nanowires as a universal platform for delivering biomolecules into living cells. Proc. Natl. Acad. Sci. 107, 1870–1875.
Sheets, M.F., Hanck, D.A., 2003. Molecular action of lidocaine on the voltage sensors of sodium channels. J. Gen. Physiol. 121, 163–175.
Spira, M., Hai, A., 2013. Multi-electrode array technologies for neuroscience and cardiology. Nat. Nanotechnol. 8, 83–94.
Tian, B., Cohen-Karni, T., Qing, Q., Duan, X., Xie, P., Lieber, C., 2010. Three-dimensional, flexible nanoscale field-effect transistors as localized bioprobes. Science 329, 830–834.
Truskey, G., Burmeister, J., Grapa, E., Reichert, W., 1992. Total internal reflection fluorescence microscopy. J. Cell Sci. 103, 491–499.
Um, E., Oh, J., Granick, S., Cho, Y., 2017. Cell migration in microengineered tumor environments. Lab Chip 17, 4171–4185.
Wang, H., Mohdavi, A., Tirrell, D., Hajimiri, A., 2012. A magnetic cell-based sensor. Lab Chip 12, 4465–4471.
Wang, Z., et al., 1998. Differential distribution of inward rectifier potassium channel transcripts in human atrium versus ventricle. Circulation 98, 2422–2428.
Xie, C., Lin, Z., Hanson, L., Cui, Y., Cui, B., 2012. Intracellular recording of action potentials by nanopillar electroporation. Nat. Nanotechnol. 7, 185–190.
Zhang, S., Zhou, Z., Gong, Q., Makielski, J., January, C., 1999. Mechanism of block and identification of the verapamil binding domain to HERG potassium channels. Circ. Res. 84, 989–998.
Zitzmann, F., Jahnke, H., Nitschke, F., Beck-Sickinger, A., Abel, B., Belder, D., Robitzki, A., 2017. A novel microfluidic microelectrode chip for a significantly enhanced monitoring of NPY-receptor activation in live mode. Lab Chip 17, 4294–4302.